Heliyon 10 (2024) e37957

Contents lists available at ScienceDirect

Heliyon

journal homepage: www.cell.com/heliyon

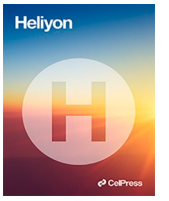

Research article

Potential mechanistic linkages of Naoluotong granules on the remission of atherosclerosis by multidimensional analysis

Shidian Zhu [a,b], Yanlin Liu [c], Wenyu Bu [a,b], Yanzi Liu [a,b], Wandi Chen [a,b], Fuming Liu [a,*]

[a] *Affiliated Hospital of Nanjing University of Chinese Medicine, Jiangsu Province Hospital of Chinese Medicine, Nanjing, 210029, China*
[b] *The First Clinical Medical College, Nanjing University of Chinese Medicine, Nanjing, 210023, China*
[c] *Affiliated Hospital of Integrated Traditional Chinese and Western Medicine, Nanjing University of Chinese Medicine, Nanjing, 210028, China*

ARTICLE INFO

Keywords:
Naoluotong granules
Atherosclerosis
Multidimensional analysis
CTSB
Mendelian randomization

ABSTRACT

Background: Naoluotong granules (NLTGs) are a medicinal formula derived from traditional Chinese medicine, which have been demonstrated to be effective in slowing down the progression of atherosclerosis (AS) through clinical practice and animal experiments. By means of multidimensional analysis, the relevant mechanism of NLTGs in delaying the progression of atherosclerosis was studied, which is conducive to its widespread adoption.

Materials and methods: In this study, data from network pharmacology and GEO database were comprehensively analysed to identify differentially expressed core cluster genes (DECCGs). Subsequently, multilevel analyses were applied to investigate the potential mechanistic linkages and causal associations of NLTGs in delaying atherosclerosis.

Results: Eight DECCGs positively correlated with atherosclerosis risk were identified, with *Polygonatum sibiricum* (Huangjing), *Hirudo nipponica* (Shuizhi), and *Ligusticum chuanxiong* (Chuanxiong) as the core drug pairs. Senkyunone, Wallichilide, and Aurantiamide were the core components. The prediction model using principal components (PC) demonstrated high accuracy and clinical relevance. The mechanisms were strongly associated with the PI3K-Akt signaling pathway, as well as the polarization of Macrophages M0 and the balanced regulation of M1/M2 types. Ultimately, elevated expression of CTSB was causally associated with increased risk of cerebral atherosclerosis (OR = 1.313; 95 % CI = 1.024–1.685; $P = 0.032$).

Conclusions: Employing multidimensional analysis, we identified core pairs, components, and targets of NLTGs. Our multilevel analysis of DECCGs enabled the construction of a clinical prediction model, highlighting CTSB as a risk target for AS. Additionally, we unveiled NLTGs' mechanisms closely tied to the polarization and regulation of macrophage, facilitating subsequent research and application.

1. Introduction

Atherosclerosis, a chronic progressive disease, is the pathological foundation of several major cardio-cerebrovascular diseases such as coronary artery disease, heart failure, and stroke. These conditions persistently impact global health and well-being, thereby

* Corresponding author.
E-mail address: doctor.liufuming@outlook.com (F. Liu).

https://doi.org/10.1016/j.heliyon.2024.e37957
Received 11 September 2024; Accepted 13 September 2024
Available online 18 September 2024

constituting a significant burden on public health worldwide [1]. The exact aetiology of AS remains unknown and dyslipidemia is considered the primary risk factor. Therefore, the primary focus in preventing and treating AS is to reduce patients' blood lipid levels and associated complications. The most commonly used medications include statins, fibrates, and new lipid regulators [2], which have achieved consistent clinical success. Although the annual mortality rate from atherosclerosis is decreasing, its incidence is still on the rise [3]. Additionally, the long-term use of lipid-lowering medications has been linked to numerous adverse effects [4], which post significant challenges to clinical practice.

In the last few years, traditional Chinese medicine (TCM) has gained traction in preventing and delaying atherosclerosis because of its multi-session, multi-pathway, and multi-target effects, along with its comparatively minimal adverse effects [5]. However, the uncertainty of active components, therapeutic mechanisms, and efficacy evaluation of its complex formulations has impeded its

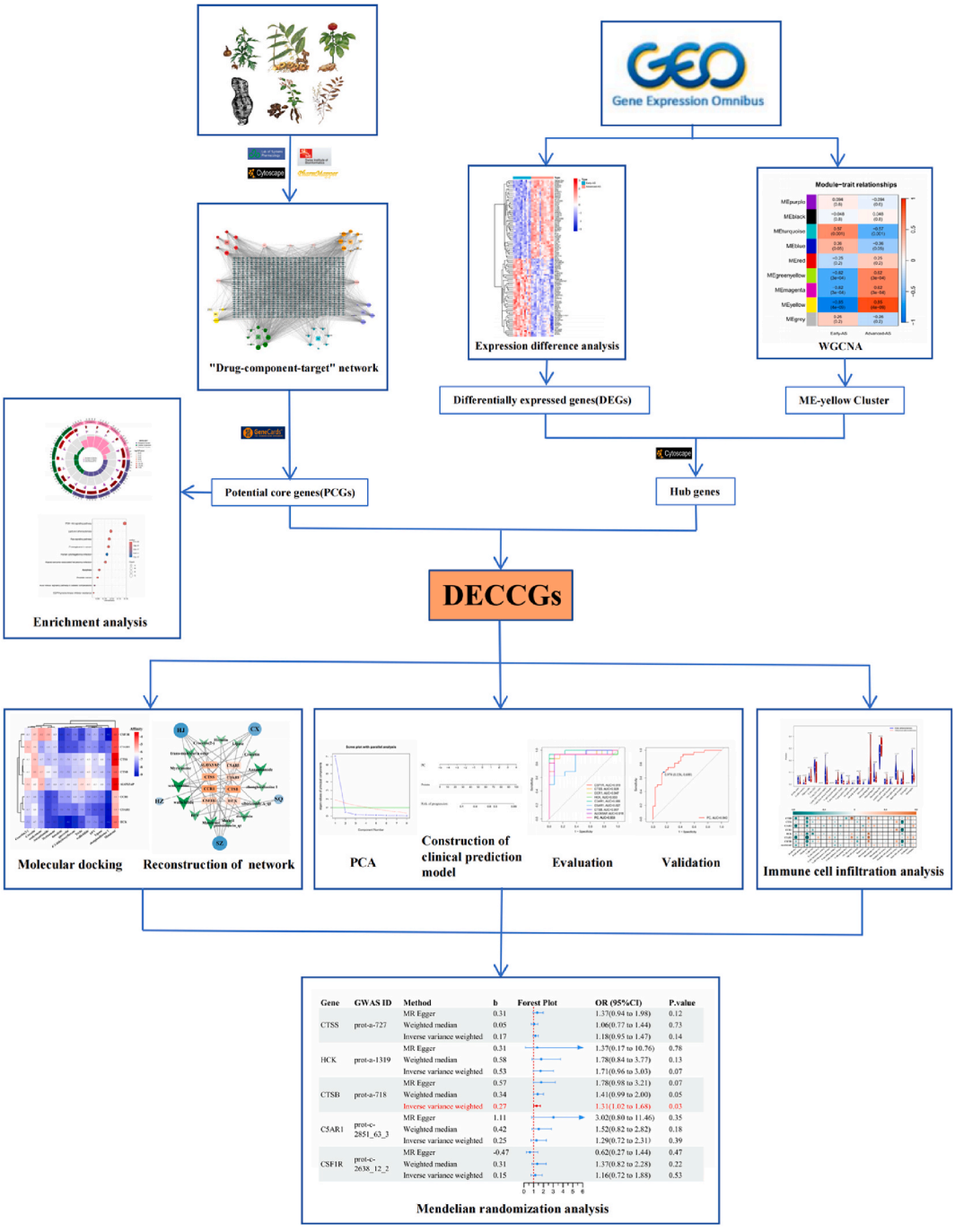

Fig. 1. Overall research flowchart.

continued popularization and application [6].

The composition of NLTGs includes *Polygonum multiflorum* (Shouwu, SW), *Polygonatum sibiricum* (Huangjing, HJ), *Sargassum fusiforme* (Haizao, HZ), *Hirudo nipponica* (Shuizhi, SZ), *Panax notoginseng* (Sanqi, SQ), and *Ligusticum chuanxiong* (Chuanxiong, CX). This formulation was developed by Professor Zhou Zhongying, a renowned expert in TCM. Significantly, both clinical theoretical discussions [7] and animal trials [8] have demonstrated its potent therapeutic effects. Based on the multimodal ultrasound system of vascular morphology-function-biomechanics, our researchers previously conducted a multicenter clinical trial to investigate the application of NLTGs for the mitigation and treatment of subclinical atherosclerosis (Sub-AS). RT-SWE and ufPWV techniques were employed to diagnose and quantitatively assess Sub-AS [9,10]. It showed that combining atorvastatin with NLTGs can more effectively lower lipid levels, alleviate inflammatory responses, improve hemorheology and vascular morphology, thereby significantly alleviating clinical symptoms in patients.

However, the preliminary research on NLTGs is still insufficient. Despite the conclusive evidence from the multicenter clinical trial, the research perspective remains relatively limited. Therefore, further study is still in need to determine the mechanisms of action. In recent years, advances in information technology have made multidimensional analysis further developed. Both multidimensional data and multilevel analysis can be used to examine NLTGs from multiple perspectives, such as gene expression, immune infiltration, modeling and genetic variation, to investigate the active components of NLTGs, the mechanisms of delaying the progression of AS and to predict the risks after treatment (Fig. 1). This will address the shortcomings of previous studies by broadening the scope of research and providing more guidance for clinical medicine [11].

2. Methods

2.1. Components and targets in Naoluotong granules

We set the retrieval deadline for all databases to cover from database establishment until February 1, 2024. Firstly, we queried the Traditional Chinese Medicine Systems Pharmacology Database and Analysis Platform (TCMSP, https://tcmsp-e.com/tcmsp.php) [12] for components of these herbs, with screening settings configured to OB $\geq$ 30 % and DL $\geq$ 0.18. The search keywords were these herbs' Chinese names: "Shouwu", "Huangjing", "Haizao", "Shuizhi", and "Sanqi". If the TCMSP database has no relevant herbs included, we utilized the HERB database (http://herb.ac.cn/) [13] for the query and SwissADME (http://www.swissadme.ch) [14] for activity screening, with "GI absorption" defined "High" and at least three "Druglikeness" reached "Yes". Subsequently, we retrieved concerned literatures to filter out the components that did not meet the above criteria, whereas the ones that did have potential research value announced in literatures could still be included in subsequent analyses [15];[16]. Finally, the Swiss Target Prediction protein database (http://www.swisstargetprediction.ch/) [17] was used to obtain the targets of active components. Those that could not be predicted due to excessively long SMILES were analysed by the Pharmmapper platform (https://www.lilab-ecust.cn/pharmmapper/) [18], with the species restricted to *Homo sapiens*.

2.2. Construction of network

We utilized Cytoscape 3.7.1 to construct a "Drug-component-target" network with drugs, components and related targets as nodes and their interrelationships as edges. We further performed topological analysis on the network with the node degree $\geq$100 taken as the condition to preliminarily screen the main components of the network.

2.3. Acquisition and enrichment analysis of PCGs

The search term "Atherosclerosis" was selected to collect AS-related targets from the GeneCards database (https://www.genecards.org/) [19]. These targets were then intersected with drug component targets to obtain Potential Core Genes (PCGs), which may play a crucial role in the chronic development of atherosclerosis. Therefore, we employed the R programming language to acquire their biological functions and pathways through GO and KEGG enrichment analysis. This enabled us to further explore their potential roles.

2.4. Collection and adjustment of GEO samples

We searched for samples in the GEO database (https://www.ncbi.nlm.nih.gov/geo/) with the keyword "Atherosclerosis". After acquiring the gene expression and clinical data, we then used the R programming language to annotate the gene symbols and adjust the data. Finally, the different expression levels of human genes were obtained in the early and advanced stages of atherosclerosis.

2.5. Difference analysis and WGCNA of AS-related GEO data

After obtaining and processing the AS-related GEO data, we conducted a difference analysis with conditions set $|\log FC| > 1$, adj.P.Val < 0.05. We then reused this dataset and applied weighted gene co-expression network analysis (WGCNA) [20] to the candidate genes with average expression $\geq$5. The minModuleSize was set to 100, and following the neighbour-joining matrix transformation, TOM distance matrix, gene clustering, and merging of similar modules, the major module was selected for subsequent analysis.

2.6. Construction of the protein-protein interaction network for hub genes

We intersected the results of the difference analysis from the GEO database with the major module obtained from WGCNA to obtain the intersection targets and subsequently imported them into the String database (https://string-db.org) [21]. The species was configured to *Homo sapiens*, and other parameters were maintained as default to obtain the PPI network of the intersection targets. Next, we applied six topological network algorithms, including MCC, Degree, Betweenness, Closeness, MNC, and EPC, via the CytoHubba plugin to filter out the top 60 as the target genes for each algorithm. Finally, we took the intersection of the six sets to obtain the hub genes. These were then visualized using the upsets diagram. The diagram was drawn with ChiPlot (https://www.chiplot.online/) (accessed on April 12, 2024).

2.7. Expression difference analysis of DECCGs

The PCGs obtained in 2.3 were intersected with the hub genes obtained in 2.6 to acquire DECCGs. Subsequently, a heatmap was generated for visualization.

2.8. Molecular docking and reconstruction of network

We obtained 14 main components of NLTGs from the previous "drug-component-target" network and retrieved their small molecule ligand structures from Pubchem (https://pubchem.ncbi.nlm.nih.gov)[22] or the TCMSP database. The 3D protein receptor structures of DECCGs were obtained from the AlphaFold protein structure database (https://alphafold.com/) [23]. We utilized Autodock Vina for molecular docking of ligands of main components with receptors of DECCGs to explore their interactions. Combinations with the best docking affinity were selected and visualized with Pymol. To further acquire the core components and core drug pairs, we reconstructed the network in Cytoscape 3.7.1, which was sorted and filtered based on degree size subsequently.

2.9. PCA, construction and validation of clinical prediction model

The expression data of DECCGs obtained after layer-by-layer screening was imported into SPSS 25.0 for standardisation and then we performed principal component analysis (PCA). Principal components meeting eigenvalues greater than 1 and cumulative variance contribution ratio greater than 85 % were selected. With the software packages "rms" and "rmda", a nomogram model was constructed via Logistic Regression after replacing the DECCGs data with the composite scores of the principal component (PC). we then calculated receiver operating characteristic (ROC) curves and calibration curves to evaluate diagnostic efficacy.

To explore the stability and clinical utility of the model, we selected another GEO dataset for external validation. The composite score of PC was calculated according to the formula, followed by the ROC curves and decision curve analysis (DCA) curves.

2.10. Infiltration, difference, and correlation of immune cells

We used the CIBERSORT package to obtain the results of immune infiltration analysis and performed difference analysis to compare the immune cell content between the early and advanced stages. The final results were shown in the form of violin plots. We then used the R packages “reshape2”, “ggpubr”, and "ggExtra" to carry out the immune cell correlation analysis of the DECCGs and obtain the correlation coefficient.

2.11. MR analysis between DECCGs and cerebral atherosclerosis

We performed a two-sample Mendelian randomization (MR) analysis to explore the causal relationship between the characteristic genes and the risk of AS. At the beginning, SNPs of the characteristic genes were obtained from the Integrated Epidemiology Unit (IEU) database (https://gwas.mrcieu.ac.uk/) to serve as exposure factors. Considering that NLTGs are now mainly used for cerebral atherosclerosis, SNPs for cerebral atherosclerosis were obtained from FinnGen R10 (https://www.finngen.fi/fi) as outcome factors. Analyses were then performed using the "Two Sample MR" software package, with the inverse variance weighted (IVW) method used to assess the relationship between the expression level of the signature genes and the risk of cerebral atherosclerosis. We finally performed a heterogeneity test and assessed potential horizontal pleiotropy.

3. Results

3.1. Active components and effective targets

After screening the TCMSP and HERB databases, along with literature review [24,25], we finally obtained 42 eligible active components of NLTGs (Supplementary Table S1). Targets were predicted by the Swiss Target Prediction protein database and the Pharmmapper platform. After further screening and weighting, we finally selected 722 effective targets.

3.2. "Drug-component-target" network and main components

The above 6 herbs, 42 components, and 722 targets were imported into Cytoscape 3.7.1, resulting in the construction of a network containing a total of 770 nodes and 2538 edges (Supplementary Fig. S1). By setting degree ≥100 as the screening condition, these 14 components were initially considered to be the material foundation of NLTGs in delaying the progression of AS: Aurantiamide, Mandenol, Wallichilide, Crocetin(2-), Crocetin, Lipase, Quercetin, Zhonghualiaoine 1, Baicalein, 4′,5-Dihydroxyflavone, Tricin, DFV, Myricanone, Senkyunone.

3.3. Identification and enrichment analysis of PCGs

After obtaining the drug-related components and targets, we retrieved a total of 5113 AS-related targets from the GeneCards database with "Atherosclerosis" as the search term. By intersecting the drug component targets with GeneCards disease targets, we finally obtained 496 Potential core genes (PCGs). Based on initial assessments, it was determined that PCGs might play an important role in delaying the progression of AS. Therefore, we further explored the potential mechanistic linkages through GO and KEGG enrichment analysis.

Using the R programming language, we performed GO enrichment analysis on PCGs associated with the remission of AS by NLTGs. The results revealed that the molecular functions (MFs) were mainly related to protein serine/threonine kinase activity, endopeptidase activity, and protein tyrosine kinase activity, etc. The detailed results are shown in Supplementary Figs. S2A and S2B.

We selected the top 10 pathways with the most significant enrichment results from KEGG analysis (Supplementary Fig. S2C). The results showed that PCGs were mainly involved in pathways such as the PI3K-Akt signaling pathway, Lipid and atherosclerosis, and Ras signaling pathway.

3.4. Results of GEO data acquisition

After searching the GEO database with the keyword "Atherosclerosis", we finally selected two datasets to compare the differences in AS progression following reading and screening. Dataset GSE28829 contained 13 early stage lesions (intimal thickening and intimal xanthomas) and 16 advanced stage lesions (thin or thick fibrous cap atherosclerotic plaques), which were used for analyses and model construction. We then selected the dataset GSE43292, which contains 32 early stage lesions (stage I and II of the Stary classification) and 32 advanced stage lesions (stage IV and over), for external validation of the constructed model.

3.5. Difference analysis and WGCNA of GEO data

The dataset GSE28829 was processed and first analysed for differences with $|\log FC| > 1$ and adj.P.Val < 0.05. This analysis acquired a total of 198 differentially expressed genes (DEGs) between early and advanced AS. The volcano map of the difference analysis for dataset GSE28829 and the heat map for a subset of DEGs are shown in Supplementary Figs. S3A and S3B. We then used the dataset GSE28829 again for WGCNA. Following module merging (Supplementary Fig. S4A), 9 different modules were identified, as shown in Supplementary Fig. S4B.

Finally, after analysing positive correlation coefficients, the ME-yellow Cluster containing 934 genes was screened. According to the scatterplot suggestion (Supplementary Fig. S4C), Module Membership was positively correlated with Gene Significance, suggesting that the key genes in the modules were closely related to AS progression. The DEGs and ME-yellow Cluster obtained after screening and analysing the GEO data were sampled from human data, making them more reliable and clinically useful.

3.6. Hub genes screening

DEGs contain the most differentially expressed genes in the progression of AS, while the ME-yellow Cluster is a co-expressed gene module. We intersected the two sets to obtain 116 intersecting targets. After constructing the PPI network, we selected six methods for screening with CytoHubba plugin. Subsequently, the intersection of the six methods was determined, and 51 hub genes were obtained from the final screening (Supplementary Fig. S5).

Table 1
Information of DECCGs.

Gene symbol	Gene name	logFC
CTSB	Cathepsin B	1.3746
CTSS	Cathepsin S	1.7239
CCR1	C-C chemokine receptor type 1	1.5111
HCK	Tyrosine-protein kinase HCK	1.4199
C3AR1	C3a anaphylatoxin chemotactic receptor 1	1.6275
C5AR1	C5a anaphylatoxin chemotactic receptor 1	1.3334
CSF1R	Macrophage colony-stimulating factor 1 receptor	1.1847
ALOX5AP	Arachidonate 5-lipoxygenase-activating protein	1.3371

3.7. Information of DECCGs

By intersecting the PCGs identified in 3.3 with the hub genes obtained in 3.6, we finally obtained 8 DECCGs (Table 1), which exhibited high expression levels in the advanced-AS group (Supplementary Fig. S6). The DECCGs were screened through network pharmacology and human samples in a stepwise manner, and they can be considered as the core targets of NLTGs in delaying the progression of AS.

3.8. Molecular docking and reconstruction of "drug-component-target" network

To evaluate the binding of the screened components and the targets, we conducted molecular docking studies of 14 ligands of main components with 8 receptors of DECCGs via Autodock Vina. The binding results are shown in Fig. 2A and Supplementary Table S2. Our findings revealed that the affinity of most combinations was lower than −5.0 kcal/mol, indicating a relatively tight binding. Among the tested interactions, the complexes formed by zhonghualiaoine 1 and CSF1R, quercetin and HCK, as well as zhonghualiaoine 1 and HCK, demonstrated the most robust binding affinities, with a calculated docking energy of −9.2 kcal/mol. Their specific binding sites and conditions are shown in Fig. 2B and C.

To further screen the core components and core drug pairs, we reconstructed the "Drug-component-target" network (Fig. 2D). According to the Degree size ranking, *Polygonatum sibiricum* (Huangjing, HJ), *Hirudo nipponica* (Shuizhi, SZ), and *Ligusticum chuanxiong* (Chuanxiong, CX) were the core drug pairs of NLTGs. The core components are Senkyunone, Wallichilide, and Aurantiamide. The heat map of molecular docking indicates consistently low binding energies of these three components with DECCGs, providing further substantiation for this conclusion.

3.9. Clinical prediction model

To reduce the effect of multicollinearity among the 8 DECCGs, we first performed PCA. After analysis, the KMO value was 0.865

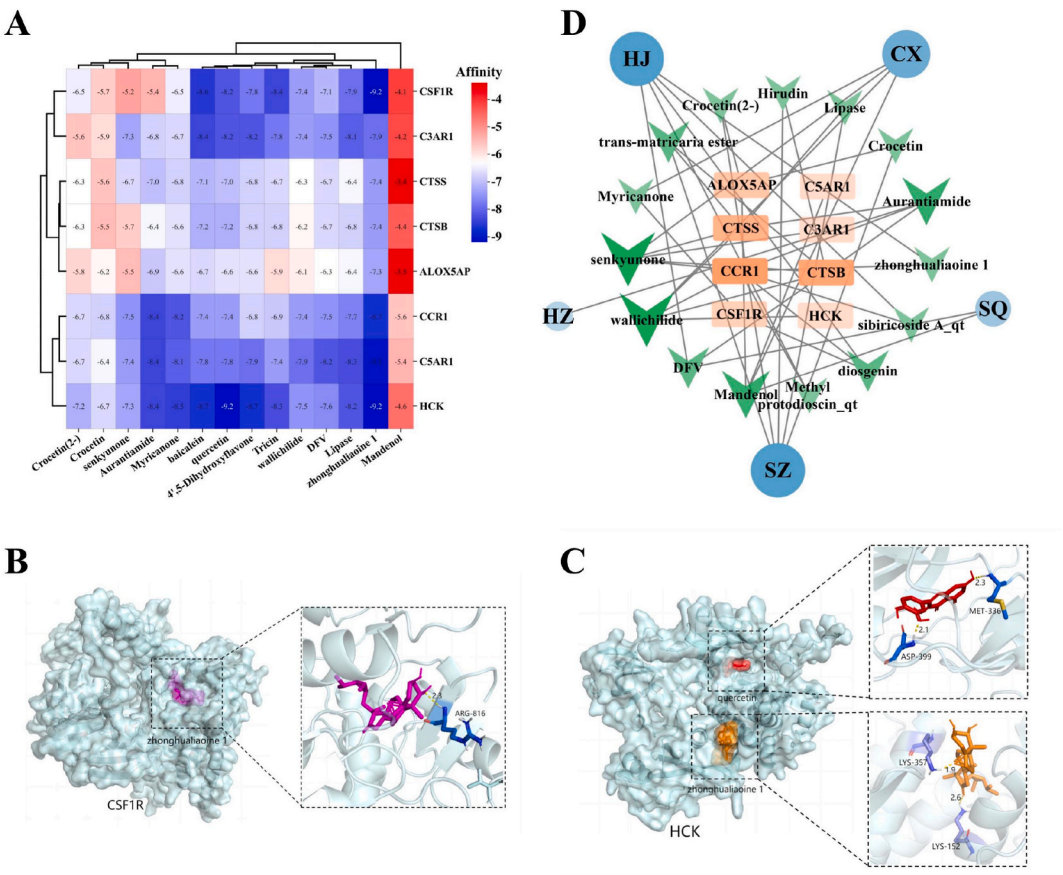

Fig. 2. (A) Heat map of molecular docking results between main components and DECCGs; (B) (C) The docking mode with the highest binding activity between main components and DECCGs (Zhonghualiaoine 1 and CSF1R, Quercetin and HCK, Zhonghualiaoine 1 and HCK); (D) Reconstruction of "Drug-component-target" network. Blue circles represent drugs, green arrows represent active components, and orange rectangles represent DECCGs. The size and color transparency of a graph are positively correlated with its degree value in the network.

and the Bartlett's sphere test resulted in $P < 0.001$, indicating that the data met the conditions for use. Finally, a principal component (PC) was obtained with eigenvalues greater than 1 and a cumulative variance contribution of 87.94 %, as shown in Fig. 3A and Supplementary Table S3. The composite score was calculated by the formula:

$$PC = 0.363 \times CSF1R + 0.363 \times HCK + 0.360 \times ALOX5AP + 0.360 \times CTSS + 0.357 \times C3AR1 + 0.357 \times CTSB + 0.349 \times CCR1 + 0.317 \times C5AR1$$

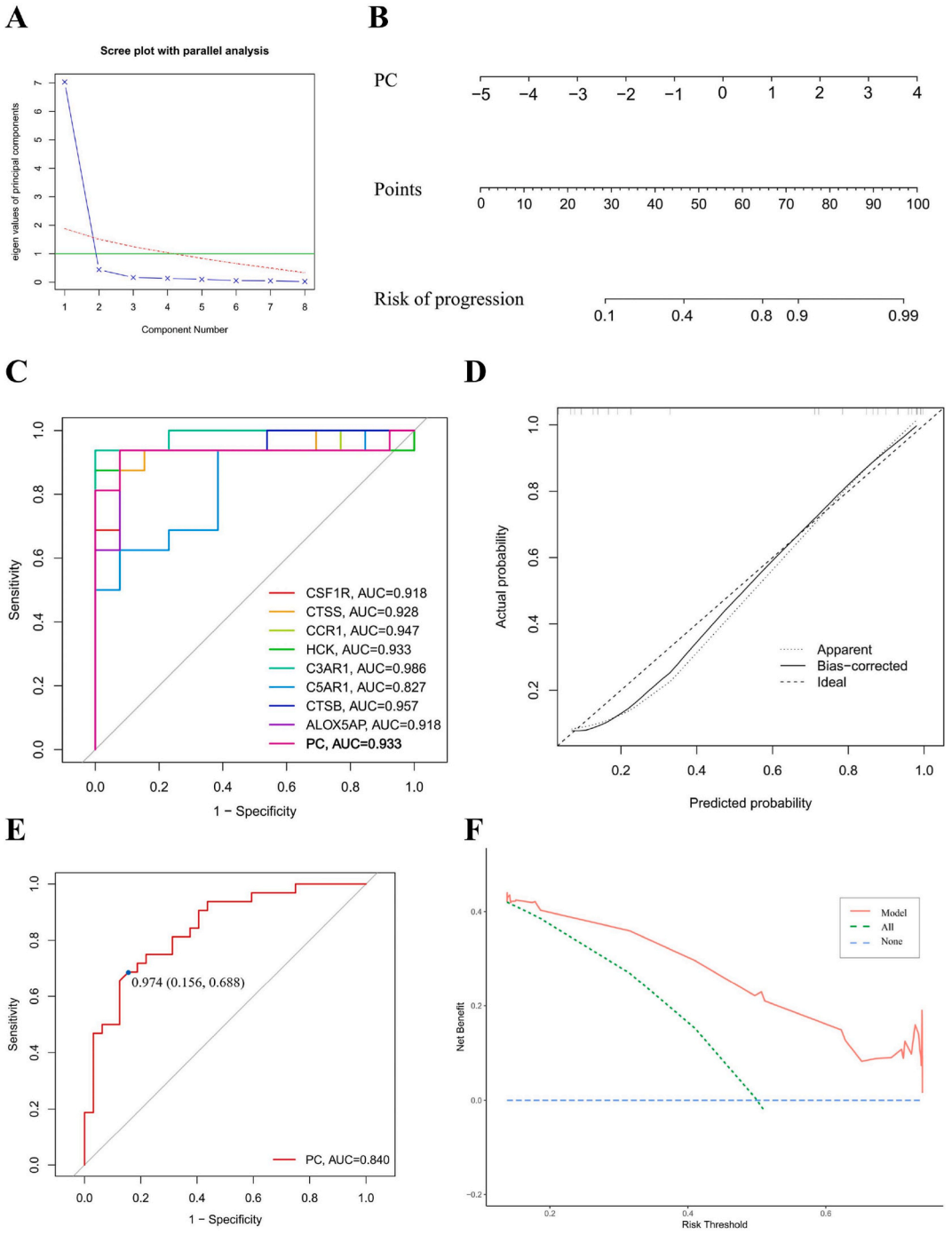

Fig. 3. (A) Scree plot of PCA; (B) Nomogram model of the principal component; (C) ROC curves to assess the diagnostic efficacy of nomogram model; (D) Calibration curves of the nomogram; (E) ROC curve of external data validation; (F) Decision curves of the nomogram.

We used the dataset GSE28829 to construct the nomogram model by employing Logistic regression through the R programming language, as shown in Fig. 3B. The diagnostic efficacy was assessed by calculating ROC curves and calibration curves. The results showed that the area under curve (AUC) was greater than 0.9 for each DECCG, except for C5AR1 (AUC = 0.827), as shown in Fig. 3C. This suggested that each DECCG had good diagnostic value. Among them, the principal component PC, which was used to construct the model instead of DECCGs, exhibited an AUC of 0.933. Moreover, the lines in the calibration curves were close to each other, confirming that the predictive model had high accuracy (Fig. 3D).

Subsequently, we selected the dataset GSE43292 for external validation of the constructed model. The composite score of PC was calculated according to the above formula, and the ROC curve was depicted, as shown in Fig. 3E. The external validation resulted in AUC = 0.840, which suggests that the constructed model was high in accuracy. Moreover, the net benefit values of the model in the DCA curves were all higher than those of None and All (Fig. 3F), which suggests that the model has good clinical utility.

3.10. Immune cell infiltration in AS

We performed difference and correlation analyses of immune cells in AS patients in order to explore the role of immune infiltration in the progression of atherosclerosis. Firstly, we performed a difference analysis to compare the immune cell content between the early and advanced stages (Fig. 4A). Statistically significant differences were observed for 7 types of immune cells, including Macrophages M0, Macrophages M2, B cells memory, T cells regulatory (Tregs), T cells gamma delta, Dendritic cells activated, and Mast cells resting. We then performed immune cell correlation analysis on the eight DECCGs (Fig. 4B). The expression of DECCGs was mainly negatively correlated with B cells naive, Plasma cells, Mast cells activated, and positively correlated with NK cells resting, Macrophages M0.

3.11. Mendelian randomization analysis

In order to explore the causal relationship between DECCGs and the risk of AS, we performed a two-sample MR analysis to reduce systematic biases such as confounders and reverse causality. From the IEU database, corresponding SNPs were obtained for 5 genes (CTSS, HCK, CTSB, C5AR1, CSF1R). From the Finnish R10 database, SNPs for cerebral atherosclerosis were obtained as an outcome factor (Fig. 5 and Supplementary Table S4).

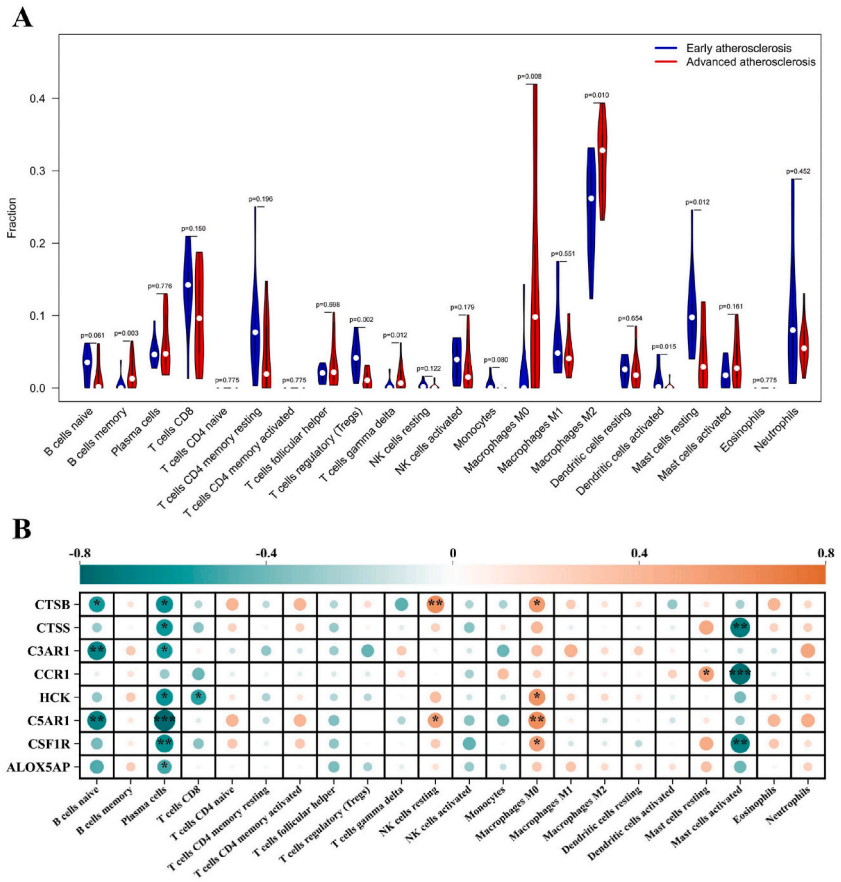

Fig. 4. (A) Violin plot of immune cell difference analysis; (B) Heat map of immune cell correlation analysis. *$p < 0.05$; **$p < 0.01$; ***$p < 0.001$.

Gene	GWAS ID	Method	b	Forest Plot	OR (95%CI)	P.value
CTSS	prot-a-727	MR Egger	0.31		1.37(0.94 to 1.98)	0.12
		Weighted median	0.05		1.06(0.77 to 1.44)	0.73
		Inverse variance weighted	0.17		1.18(0.95 to 1.47)	0.14
HCK	prot-a-1319	MR Egger	0.31		1.37(0.17 to 10.76)	0.78
		Weighted median	0.58		1.78(0.84 to 3.77)	0.13
		Inverse variance weighted	0.53		1.71(0.96 to 3.03)	0.07
CTSB	prot-a-718	MR Egger	0.57		1.78(0.98 to 3.21)	0.07
		Weighted median	0.34		1.41(0.99 to 2.00)	0.05
		Inverse variance weighted	0.27		1.31(1.02 to 1.68)	0.03
C5AR1	prot-c-2851_63_3	MR Egger	1.11		3.02(0.80 to 11.46)	0.35
		Weighted median	0.42		1.52(0.82 to 2.82)	0.18
		Inverse variance weighted	0.25		1.29(0.72 to 2.31)	0.39
CSF1R	prot-c-2638_12_2	MR Egger	-0.47		0.62(0.27 to 1.44)	0.47
		Weighted median	0.31		1.37(0.82 to 2.28)	0.22
		Inverse variance weighted	0.15		1.16(0.72 to 1.88)	0.53

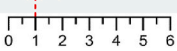

Fig. 5. Summary of Mendelian randomization analysis between five DECCGs and cerebral atherosclerosis.

Ultimately, IVW analysis showed that CTSB expression levels were associated with an increased risk of cerebral atherosclerosis (OR = 1.313; 95 % CI = 1.024–1.685; $P = 0.032$). The b values were all greater than 0 and directionally consistent after using three Mendelian randomization methods. The causal effect of CTSB on cerebral atherosclerosis is shown in Supplementary Fig. S7A, while the causal effect of a single SNP is shown in Supplementary Fig. S7B. Leave-one-out analysis showed that the MR analysis results of the remaining SNPs remained relatively robust after the single removal of a SNP (Supplementary Fig. S7C). The scatter of the funnel plot was approximately symmetric, which suggested lower overall heterogeneity (Supplementary Fig. S7D).

We conducted a test for heterogeneity, and both the IVW method ($P = 0.58$) and MR-Egger regression ($P = 0.60$) yielded P-values greater than 0.05, suggesting no heterogeneity. As for the test of pleiotropy, both MR-Egger regression ($P = 0.29$) and MR-PRESSO analysis ($P = 0.62$) suggested that the presence of horizontal pleiotropy was not considered.

4. Discussion

4.1. *Naoluotong granules on the progression of atherosclerosis*

Regarding the causes of chronic progression of atherosclerosis, Professor Zhou Zhongying believes that from the perspective of TCM, the key point is the deficiency of the liver and kidney, with phlegm and blood stasis at the centre of the pathology. Therefore, the principle of treatment in TCM is to nourish the kidney and liver, and to eliminate phlegm and blood stasis. Based on this principle, Professor Zhou created Naoluotong Granules.

After our screening of Naoluotong Granules by multidimensional analysis, *Polygonatum sibiricum* (Huangjing), *Hirudo nipponica* (Shuizhi), and *Ligusticum chuanxiong* (Chuanxiong) were identified as the core drug pairs. Firstly, Huangjing has the effect of benefiting the kidney and nourishing yin. Studies have shown that polysaccharides from Polygonatum sibiricum can lower blood lipids and inhibit the formation of foam cell, thus exerting anti-atherosclerosis effects [26]. Secondly, Chuanxiong can promote the circulation of blood and flow of qi. The two most important components of NLTGs after screening, senkyunone and wallichilide, are derived from Chuanxiong. Numerous studies have been conducted on its anti-atherosclerotic mechanisms currently. Generally speaking, the main effects include anti-platelet aggregation [27], regulation of blood lipids [28], and so on. Thirdly, Shuizhi has an extremely strong blood-activating effect. Its main active component, hirudin, is the strongest natural specific inhibitor of thrombin found to date [29, 30]. A network meta-analysis also indicated that Chinese patent drugs containing Shuizhi have good efficacy in the treatment of AS without increasing adverse effects [31]. These three herbs, as a core pair, play the most important role in slowing down the progression of atherosclerosis in NLTGs.

Eight DECCGs (CTSB, CTSS, C3AR1, C5AR1, CCR1, CSF1R, HCK, ALOX5AP) were derived from the target prediction of herbal components and the GEO database. They underwent topological analysis, difference analysis, and WGCNA screening. Furthermore, they have subsequently been demonstrated to be the most central targets of NLTGs in delaying AS progression through multiple levels and perspectives. Notably, CTSB and CTSS are both histone proteases that share the same structural scaffolding. The expression of Cathepsin increases in the vascular endothelium, myocardial fibers, and blood of AS patients, affecting the activation of inflammatory molecules, cell migration, and neovascularization [32], which is expected to be biomarkers and diagnostic imaging tools [33]. Our Mendelian randomization studies have, for the first time, revealed a strong causal relationship between CTSB and cerebral atherosclerosis (OR = 1.313; 95 % CI = 1.024–1.685; $P = 0.032$), which provides strong support for the above point. Both C3AR1 and C5AR1 are anaphylatoxin chemotactic receptor, which are closely related to pathophysiological processes such as immune response

regulation and lipid catabolism. Therefore, they are also correlated with the progression of atherosclerosis [34,35]. Further information about the remaining targets can be found in the corresponding literature. For example, activation of CCR1 was found to lead to macrophage migration and vascular inflammation, thus promoting atherosclerosis [36].

4.2. Application, analysis and screening of human sample data

For data sources, we utilized the GEO database for analysis and screening, complementing the classical network pharmacology methods. Genes screened from human samples are characterized by higher accuracy and clinical relevance [11].

For data analysis, we conducted both difference analysis and WGCNA of GEO data to explore the modular relationship between differentially expressed genes. The final hub genes, obtained after double screening and topological analysis, exhibit dual characteristics of differential expression and high synergy in the progression of atherosclerosis. These characteristics can reflect the complex linkage of the action targets of Chinese medicine formulas.

For case selection, we opted for the early-advanced AS group instead of the traditional healthy-disease group, considering the chronic progressive nature of AS. The pathological progression of AS may have started gradually in youth. This is a gradual and continuous process, which makes it difficult to differentiate a perfectly healthy population by a certain indicator (e.g. carotid intima-media thickness). It is critical to assess the risk of progression of early lesions once they have been identified by imaging techniques. Therefore, the selection of such human sample data is more clinically relevant.

4.3. Construction and validation of the clinical prediction model

When constructing the clinical prediction model, principal component analysis was initially performed on the data. The reason is that the modular genes screened by WGCNA are closely related and have multicollinearity, which may lead to a deviation from clinical practice in the conclusion. After dimensionality reduction via principal component analysis, the cumulative variance contribution rate reached 87.94 %, indicating a small information loss. The accuracy of the prediction model was confirmed by analyzing the ROC and calibration curves of the principal component. Subsequently, its accuracy and practicality were externally validated through the analysis of ROC and DCA curves with an independent dataset. By calculating the comprehensive score of the principal component with a specified formula and interpreting it via a nomogram, the current risk of AS progression can be assessed.

4.4. Immune cell infiltration

Through difference and correlation analyses of immune cells, it was determined that the expression of Macrophages M0 between early-AS and advanced-AS differed significantly ($P = 0.008$) and was positively correlated with DECCGs. Macrophages M0, which are in an unactivated and immature state, function primarily in phagocytosis and the removal of cell debris. Upon stimulation with agents such as IFN-γ and LPS, they can be induced to polarize into Macrophages M1, which secrete numerous inflammatory cytokines at the early stage of inflammatory response, thereby promoting the progression of AS. Activation by IL-4 and IL-10 can induce polarization into Macrophages M2, which attenuates the inflammatory response and promotes tissue repair and regeneration [37]. Therefore, balanced polarization of Macrophages M1/M2 is critical for regulating the body's inflammatory response.

In the current analysis, Macrophages M2 were found to be more highly expressed in advanced-AS ($P = 0.010$). This expression may be attributed to the body's response modulation during long-term chronic inflammation, which promotes tissue self-repair and remodeling for plaque stabilization [38], or to benign interventions with common anti-plaque medications such as statins [39]. Enrichment analysis of PCGs was performed, and the results indicated that the PCGs mainly influence the PI3K-Akt signaling pathway. Numerous studies have demonstrated that the PI3K-Akt signaling pathway plays a crucial role in regulating macrophage dual-property inflammation [40–42]. Therefore, the mechanisms by which NLTGs delay the progression of atherosclerosis are closely related to the polarization of Macrophages M0 and the balanced regulation of M1/M2.

4.5. The advantages and shortcomings of this study

This study has certain advantages over previous. Firstly, the preliminary work comprising multicenter clinical trials and extensive clinical practice verification of NLTGs, while research into the related mechanisms has not been systematically conducted. Through multidimensional analysis, this study has addressed these gaps. The screening of core drug pairs can facilitate the refinement of Chinese medicine formulas. At the same time, acquiring core components advances further in-depth research on NLTGs and facilitates drug development. Furthermore, selecting core targets aids in elucidating relevant mechanisms from a deeper perspective and identifying biomarkers with diagnostic value.

Secondly, in contrast to the traditional emphasis on differences between normal individuals and AS patients, our study concentrates on conducting difference analysis between early and advanced AS groups. From a clinical perspective, patients frequently seek medical attention upon plaque discovery to prevent further development. This research holds greater relevance to clinical practice and offers higher clinical practical value.

Thirdly, the formulation of TCM should focus on not only the simple combinations of herbs but also the relationship network among different components and targets. Consequently, we integrated GEO difference analysis with WGCNA module screening to identify targets exhibiting both expression differences and synergistic effects.

Finally, under the guidance of current ultrasound technology, it remains challenging to identify the early stage and quantify the

risks based on arterial intima-media thickening or plaque detection alone. Screening DECCGs and constructing models can aid in evaluating drug efficacy, quantifying and identifying early risks in high-risk populations, and may also facilitate prognosis assessment. Particularly for CTSB, the evidence is robust after conducting Mendelian randomization analysis for causal inference.

Despite the above advantages, there are some shortcomings in this study. While human sample data has been included, collaborative validation in vivo and in vitro experiments is still necessary following multidimensional analysis and screening [43]. Moreover, while multidimensional analysis and screening methods emphasize organizational network relationships, they may overlook isolated important components and drug doses.

5. Conclusions

Following multidimensional analysis of NLTGs, we identified the corresponding core drug pairs, core components, and core targets. Subsequently, we conducted further analysis of DECCGs from multiple levels. Ultimately, a potent risk target for predicting the progression of AS, CTSB, was identified, and a corresponding clinical prediction model was constructed, which will facilitate further research and application of NLTGs.

Data availability statement

The names and access numbers of the relevant datasets mentioned in this study can be found in the article/supplementary material. The relevant raw data can be obtained in online repositories.

Sources of funding

The author/s declare financial support was received for the research, authorship, and/or publication of this article. The Key Project of Jiangsu Provincial Health and Health Commission (ZD2022001); The Key Planning Project for the Science and Technology Development of Traditional Chinese Medicine of Jiangsu Province (ZD201906); The Natural Science Foundation Project of Nanjing University of Chinese Medicine (XZR2021020); The Six Talent Peaks Project in Jiangsu Province (TD-SWYY-069).

CRediT authorship contribution statement

Shidian Zhu: Conceptualization, Data curation, Formal analysis, Investigation, Methodology, Resources, Software, Visualization, Writing – original draft, Writing – review & editing. **Yanlin Liu:** Data curation, Project administration, Supervision. **Wenyu Bu:** Conceptualization, Writing – review & editing. **Yanzi Liu:** Writing – review & editing. **Wandi Chen:** Writing – review & editing. **Fuming Liu:** Funding acquisition, Project administration, Writing – review & editing.

Declaration of competing interest

The authors declare that they have no known competing financial interests or personal relationships that could have appeared to influence the work reported in this paper.

Appendix A. Supplementary data

Supplementary data to this article can be found online at https://doi.org/10.1016/j.heliyon.2024.e37957.

References

[1] K.L.K. Kobiyama, Atherosclerosis a chronic inflammatory disease with an autoimmune component, Circ. Res.: J. Am. Heart Assoc. 123 (10) (2018).
[2] Robert M. Stoekenbroek, Caroline Bruikman, S, et al., New drugs for atherosclerosis, Can. J. Cardiol. 33 (3) (2017) 350–357.
[3] P. Song, Z. Fang, H. Wang, Y. Cai, K. Rahimi, Y. Zhu, F.G.R. Fowkes, F.J.I. Fowkes, I. Rudan, Global and regional prevalence, burden, and risk factors for carotid atherosclerosis: a systematic review, meta-analysis, and modelling study, Lancet Global Health 8 (5) (2020) e721–e729, https://doi.org/10.1016/S2214-109X(20)30117-0.
[4] J.M. Backes, J.F. Ruisinger, C.A. Gibson, P.M. Moriarty, Statin-associated muscle symptoms-Managing the highly intolerant, Journal of clinical lipidology 11 (1) (2017) 24–33, https://doi.org/10.1016/j.jacl.2017.01.006.
[5] W. Wang, H. Li, Y. Shi, J. Zhou, G.J. Khan, J. Zhu, F. Liu, H. Duan, L. Li, K. Zhai, Targeted intervention of natural medicinal active ingredients and traditional Chinese medicine on epigenetic modification: possible strategies for prevention and treatment of atherosclerosis, Phytomedicine : international journal of phytotherapy and phytopharmacology 122 (2024) 155139, https://doi.org/10.1016/j.phymed.2023.155139.
[6] G.S. Wu, H.K. Li, W.D. Zhang, Metabolomics and its application in the treatment of coronary heart disease with traditional Chinese medicine, Chin. J. Nat. Med. 17 (5) (2019) 321–330, https://doi.org/10.1016/S1875-5364(19)30037-8.
[7] Z.Y. Zhou, M.W. Jin, Q. Gu, et al., Theoretical exploration into treatment of atherosclerosis by nourishing kidney and liver, resolving phlegm and removing blood stasis, J Nanjing Univ Tradit Chin Med. (03) (2002) 137–139.
[8] S.H. Yan, Q.Y. Li, Z.T. Lu, et al., Effects of Naoluotong granules on NF-κB and PPAR-γ in vascular tissue of atherosclerotic mice, J. Tradit. Chin. Med. 55 (12) (2014) 1047–1050, https://doi.org/10.13288/j.11-2166/r.2014.12.016.

[9] F.S. Pan, L. Yu, J. Luo, R.D. Wu, M. Xu, J.Y. Liang, Y.L. Zheng, X.Y. Xie, Carotid artery stiffness assessment by ultrafast ultrasound imaging: feasibility and potential influencing factors, J. Ultrasound Med. : official journal of the American Institute of Ultrasound in Medicine 37 (12) (2018) 2759–2767, https://doi.org/10.1002/jum.14630.

[10] Z.Q. Zhu, L.S. Chen, H. Wang, F.M. Liu, Y. Luan, L.L. Wu, N. Liu, P. Wang, H. Huang, Carotid stiffness and atherosclerotic risk: non-invasive quantification with ultrafast ultrasound pulse wave velocity, Eur. Radiol. 29 (3) (2019) 1507–1517, https://doi.org/10.1007/s00330-018-5705-7.

[11] Y. Liu, X. Cui, X. Zhang, Z. Xie, W. Wang, J. Xi, Y. Xie, Exploring the potential mechanisms of Tongmai Jiangtang capsules in treating diabetic nephropathy through multi-dimensional data, Front. Endocrinol. 14 (2023) 1172226, https://doi.org/10.3389/fendo.2023.1172226.

[12] J. Ru, P. Li, J. Wang, W. Zhou, B. Li, C. Huang, P. Li, Z. Guo, W. Tao, Y. Yang, X. Xu, Y. Li, Y. Wang, L. Yang, TCMSP: a database of systems pharmacology for drug discovery from herbal medicines, J. Cheminf. 6 (2014) 13, https://doi.org/10.1186/1758-2946-6-13.

[13] S. Fang, L. Dong, L. Liu, J. Guo, L. Zhao, J. Zhang, D. Bu, X. Liu, P. Huo, W. Cao, Q. Dong, J. Wu, X. Zeng, Y. Wu, Y. Zhao, HERB: a high-throughput experiment- and reference-guided database of traditional Chinese medicine, Nucleic Acids Res. 49 (D1) (2021) D1197–D1206, https://doi.org/10.1093/nar/gkaa1063.

[14] A. Daina, O. Michielin, V. Zoete, SwissADME: a free web tool to evaluate pharmacokinetics, drug-likeness and medicinal chemistry friendliness of small molecules, Sci. Rep. 7 (2017) 42717, https://doi.org/10.1038/srep42717.

[15] K. Zhai, H. Duan, W. Wang, S. Zhao, G.J. Khan, M. Wang, Y. Zhang, K. Thakur, X. Fang, C. Wu, J. Xiao, Z. Wei, Ginsenoside Rg1 ameliorates blood-brain barrier disruption and traumatic brain injury via attenuating macrophages derived exosomes miR-21 release, Acta Pharm. Sin. B 11 (11) (2021) 3493–3507, https://doi.org/10.1016/j.apsb.2021.03.032.

[16] K.F. Zhai, J.R. Zheng, Y.M. Tang, F. Li, Y.N. Lv, Y.Y. Zhang, Z. Gao, J. Qi, B.Y. Yu, J.P. Kou, The saponin D39 blocks dissociation of non-muscular myosin heavy chain IIA from TNF receptor 2, suppressing tissue factor expression and venous thrombosis, Br. J. Pharmacol. 174 (17) (2017) 2818–2831, https://doi.org/10.1111/bph.13885.

[17] A. Daina, O. Michielin, V. Zoete, SwissTargetPrediction: updated data and new features for efficient prediction of protein targets of small molecules, Nucleic Acids Res. 47 (W1) (2019) W357–W364, https://doi.org/10.1093/nar/gkz382.

[18] X. Wang, Y. Shen, S. Wang, S. Li, W. Zhang, X. Liu, L. Lai, J. Pei, H. Li, PharmMapper 2017 update: a web server for potential drug target identification with a comprehensive target pharmacophore database, Nucleic Acids Res. 45 (W1) (2017) W356–W360, https://doi.org/10.1093/nar/gkx374.

[19] M. Safran, N. Rosen, M. Twik, R. Barshir, T.I. Stein, D. Dahary, et al., The genecards suite, J. Mol. Biol. (2021), https://doi.org/10.1007/978-981-16-5812-9_2, 433-11.

[20] P. Langfelder, S. Horvath, WGCNA: an R package for weighted correlation network analysis, BMC Bioinf. 9 (2008) 559, https://doi.org/10.1186/1471-2105-9-559.

[21] D. Szklarczyk, A.L. Gable, K.C. Nastou, D. Lyon, R. Kirsch, S. Pyysalo, N.T. Doncheva, M. Legeay, T. Fang, P. Bork, L.J. Jensen, C. von Mering, The STRING database in 2021: customizable protein-protein networks, and functional characterization of user-uploaded gene/measurement sets, Nucleic Acids Res. 49 (D1) (2021) D605–D612, https://doi.org/10.1093/nar/gkaa1074.

[22] S. Kim, J. Chen, T. Cheng, A. Gindulyte, J. He, S. He, et al., PubChem 2023 update, Nucleic Acids Res. 51 (D1) (2023) D1373–D1380, https://doi.org/10.1093/nar/gkac956.

[23] M. Varadi, S. Anyango, M. Deshpande, S. Nair, C. Natassia, G. Yordanova, D. Yuan, O. Stroe, G. Wood, A. Laydon, A. Žídek, T. Green, K. Tunyasuvunakool, S. Petersen, J. Jumper, E. Clancy, R. Green, A. Vora, M. Lutfi, M. Figurnov, S. Velankar, AlphaFold Protein Structure Database: massively expanding the structural coverage of protein-sequence space with high-accuracy models, Nucleic Acids Res. 50 (D1) (2022) D439–D444, https://doi.org/10.1093/nar/gkab1061.

[24] A. Greinacher, N. Lubenow, Recombinant hirudin in clinical practice: focus on lepirudin, Circulation 103 (10) (2001) 1479–1484, https://doi.org/10.1161/01.cir.103.10.1479.

[25] S.L. Luo, L.Z. Dang, J.F. Li, C.G. Zou, K.Q. Zhang, G.H. Li, Biotransformation of saponins by endophytes isolated from Panax notoginseng, Chem. Biodivers. 10 (11) (2013) 2021–2031, https://doi.org/10.1002/cbdv.201300005.

[26] J.X. Yang, S. Wu, X.L. Huang, X.Q. Hu, Y. Zhang, Hypolipidemic activity and antiatherosclerotic effect of polysaccharide of Polygonatum sibiricum in rabbit model and related cellular mechanisms, Evid. base Compl. Alternative Med. : eCAM 2015 (2015) 391065, https://doi.org/10.1155/2015/391065.

[27] L. Li, H. Chen, A. Shen, Q. Li, Y. Chen, J. Chu, L. Liu, J. Peng, K. Chen, Ligustrazine inhibits platelet activation via suppression of the Akt pathway, Int. J. Mol. Med. 43 (1) (2019) 575–582, https://doi.org/10.3892/ijmm.2018.3970.

[28] J. Chen, J. Tian, H. Ge, R. Liu, J. Xiao, Effects of tetramethylpyrazine from Chinese black vinegar on antioxidant and hypolipidemia activities in HepG2 cells, Food Chem. Toxicol. : an international journal published for the British Industrial Biological Research Association 109 (Pt 2) (2017) 930–940, https://doi.org/10.1016/j.fct.2016.12.017.

[29] Y. Xie, F. Lan, J. Zhao, W. Shi, Hirudin improves renal interstitial fibrosis by reducing renal tubule injury and inflammation in unilateral ureteral obstruction (UUO) mice, Int. Immunopharm. 81 (2020) 106249, https://doi.org/10.1016/j.intimp.2020.106249.

[30] W.F. Lu, W. Mo, Z. Liu, W.G. Fu, D.Q. Guo, Y.Q. Wang, H.Y. Song, The antithrombotic effect of a novel hirudin derivative after reconstruction of carotid artery in rabbits, Thromb. Res. 126 (4) (2010) e339–e343, https://doi.org/10.1016/j.thromres.2010.03.022.

[31] Q.Q. Han, Z.Y. Wen, Q. Lyu, Y.Y. Pan, Zhongguo Zhong yao za zhi = Zhongguo zhongyao zazhi = China journal of Chinese materia medica 48 (1) (2023) 234–246, https://doi.org/10.19540/j.cnki.cjcmm.20221018.501.

[32] X. Zhang, S. Luo, M. Wang, G.P. Shi, Cysteinyl cathepsins in cardiovascular diseases, Biochimica et biophysica acta. Proteins and proteomics 1868 (4) (2020) 140360, https://doi.org/10.1016/j.bbapap.2020.140360.

[33] X.W. Cheng, M. Narisawa, H. Wang, L. Piao, Overview of multifunctional cysteinyl cathepsins in atherosclerosis-based cardiovascular disease: from insights into molecular functions to clinical implications, Cell Biosci. 13 (1) (2023) 91, https://doi.org/10.1186/s13578-023-01040-4.

[34] D. Ricklin, J.D. Lambris, Complement in immune and inflammatory disorders: pathophysiological mechanisms, Journal of immunology (Baltimore, Md 190 (8) (2013) 3831–3838, https://doi.org/10.4049/jimmunol.1203487, 1950.

[35] R. Li, L.G. Coulthard, M.C. Wu, S.M. Taylor, T.M. Woodruff, C5L2: a controversial receptor of complement anaphylatoxin, C5a, Faseb. J. : official publication of the Federation of American Societies for Experimental Biology 27 (3) (2013) 855–864, https://doi.org/10.1096/fj.12-220509.

[36] J. Jehle, B. Schöne, S. Bagheri, E. Avraamidou, M. Danisch, I. Frank, P. Pfeifer, L. Bindila, B. Lutz, D. Lütjohann, A. Zimmer, G. Nickenig, Elevated levels of 2-arachidonoylglycerol promote atherogenesis in ApoE-/- mice, PLoS One 13 (5) (2018) e0197751, https://doi.org/10.1371/journal.pone.0197751.

[37] C.D. Mills, M1 and M2 macrophages: oracles of health and disease, Crit. Rev. Immunol. 32 (6) (2012) 463–488, https://doi.org/10.1615/critrevimmunol.v32.i6.10.

[38] G. Chinetti-Gbaguidi, M. Daoudi, M. Rosa, M. Vinod, L. Louvet, C. Copin, M. Fanchon, J. Vanhoutte, B. Derudas, L. Belloy, S. Haulon, C. Zawadzki, S. Susen, Z. A. Massy, J. Eeckhoute, B. Staels, Human alternative macrophages populate calcified areas of atherosclerotic lesions and display impaired RANKL-induced osteoclastic bone resorption activity, Circ. Res. 121 (1) (2017) 19–30, https://doi.org/10.1161/CIRCRESAHA.116.310262.

[39] X. Zhang, Y. Qin, X. Wan, H. Liu, C. Lv, W. Ruan, L. He, L. Lu, X. Guo, Rosuvastatin exerts anti-atherosclerotic effects by improving macrophage-related foam cell formation and polarization conversion via mediating autophagic activities, J. Transl. Med. 19 (1) (2021) 62, https://doi.org/10.1186/s12967-021-02727-3.

[40] A. Arranz, C. Doxaki, E. Vergadi, Y. Martinez de la Torre, K. Vaporidi, E.D. Lagoudaki, E. Ieronymaki, A. Androulidaki, M. Venihaki, A.N. Margioris, E. N. Stathopoulos, P.N. Tsichlis, C. Tsatsanis, Akt1 and Akt2 protein kinases differentially contribute to macrophage polarization, Proceedings of the National Academy of Sciences of the United States of America 109 (24) (2012) 9517–9522, https://doi.org/10.1073/pnas.1119038109.

[41] E. Vergadi, E. Ieronymaki, K. Lyroni, K. Vaporidi, C. Tsatsanis, Akt signaling pathway in macrophage activation and M1/M2 polarization, Journal of immunology (Baltimore, Md. : 1950) 198 (3) (2017) 1006–1014, https://doi.org/10.4049/jimmunol.1601515.

[42] V.R. Babaev, K.E. Hebron, C.B. Wiese, C.L. Toth, L. Ding, Y. Zhang, J.M. May, S. Fazio, K.C. Vickers, M.F. Linton, Macrophage deficiency of Akt2 reduces atherosclerosis in Ldlr null mice, J. Lipid Res. 55 (11) (2014) 2296–2308, https://doi.org/10.1194/jlr.M050633.

[43] J. Zeng, C. Lai, J. Luo, L. Li, Functional investigation and two-sample Mendelian randomization study of neuropathic pain hub genes obtained by WGCNA analysis, Front. Neurosci. 17 (2023) 1134330, https://doi.org/10.3389/fnins.2023.1134330.